CARBON 72 (2014) 402–409

Available at www.sciencedirect.com

ScienceDirect

journal homepage: www.elsevier.com/locate/carbon

Diversity of ultrafast hot-carrier-induced dynamics and striking sub-femtosecond hot-carrier scattering times in graphene

Ke Chen [a], *Huihui Li* [a], *Lai-Peng Ma* [b], *Wencai Ren* [b], *Ting-Fung Chung* [c], *Hui-Ming Cheng* [b], *Yong P. Chen* [c], *Tianshu Lai* [a,*]

[a] *State-Key Laboratory of Optoelectronic Materials and Technologies, School of Physics and Engineering, Sun Yat-Sen University, Guangzhou, Guangdong 510275, China*

[b] *Shenyang National Laboratory for Material Science, Institute of Metal Research, Chinese Academy of Science, Shenyang 110016, China*

[c] *Department of Physics, Purdue University, W. Lafayette, IN 47907, USA*

ARTICLE INFO

Article history:
Received 10 August 2013
Accepted 12 February 2014
Available online 18 February 2014

ABSTRACT

We study ultrafast dynamics in graphene grown by chemical vapor deposition, which presents a positive peak followed by a negative slow recovery process, and is different from the fully positive or negative dynamics reported. We discuss the diversity of ultrafast dynamics. A dynamic model of differential optical conductivity is developed to simulate ultrafast dynamics. It is found that the diversity of ultrafast dynamics originates from multiple parameter dependence. The appearance of ultrafast dynamics is mainly determined by the position of probed level with respect to static Fermi energy and/or momentum scattering time. The dynamic model is used to best fit the observed ultrafast dynamics to retrieve dynamic time constants. The thermalizing and cooling times of optical phonons are found consistent with the reported values, but a striking sub-femtosecond momentum scattering time and a sub-picosecond time of electron–hole recombination are obtained. The sub-femtosecond scattering time is much shorter than several to a few hundred femtoseconds accepted currently.

1. Introduction

The development of graphene-based high speed electronic devices requires the understanding of ultrafast carrier dynamic processes in graphene. Many researches reported on the ultrafast carrier dynamics in mono- and few-layer graphene, and revealed rich and diverse ultrafast dynamics. Dawlaty et al. first studied the ultrafast carrier dynamics in few-layer epitaxial graphene grown on 6H-SiC by thermal decomposition of SiC surface at high temperatures using near-infrared femtosecond pump–probe differential transmission spectroscopy [1], and found a pure absorption-saturated ultrafast dynamics, that is a fully positive differential transmission dynamics (DTD). Thereafter, many researches also reported on similar fully positive DTDs in few-layer graphene grown on 6H-SiC by thermal decomposition of SiC surface and grown by chemical vapor deposition (CVD) [2], in solution-processable few-layer graphene oxide and reduced graphene oxide [3], and in mono-layer graphene on SiO_2 grown by CVD [4]. Meanwhile, a fully negative

* *Corresponding author:* Fax: +86 2084037423.
E-mail address: stslts@mail.sysu.edu.cn (T. Lai).
http://dx.doi.org/10.1016/j.carbon.2014.02.039
0008-6223/

differential reflectivity dynamics (DRD) was also reported in mono-layer graphene grown on 6H-SiC by thermal decomposition of 6H-SiC [5], which is equivalent to a fully positive DTD. In contrast, another researchers reported on fully negative DTD, that is absorption-enhanced dynamics, in mono- and a few-layer graphene grown on 6H-SiC [6], few-layer graphene grown on 6H-SiC [7], a few-layer graphene grown on 4H-SiC [8], and mono- and a few-layer exfoliated graphene on a Si substrate [9]. Similarly, a fully positive DRD was also observed in mono-layer graphene transferred on glass [10] and MgO [11] substrates grown by CVD, which was equivalent to a fully negative DTD. In addition, complex probe-wavelength-dependent evolution of DTD was also reported [12–14]. Shang et al. [12,13] and Breusing et al. [14] studied the ultrafast carrier dynamics of CVD-grown a mono- and few-layer graphene transferred on quartz substrates [12,13] and exfoliated monolayer graphene on mica substrates [14], respectively and found that DTD was fully positive as the wavelength of probe (probed level) was longer (lower). However, the dynamics was evolved into an initial positive peak followed by a slow negative recovery dynamics as the wavelength of probe (probed level) decreased (increased). Sun et al. [15] investigated the ultrafast carrier dynamics of bi-layer graphene grown on 4H-SiC by thermal desorption of Si, and found that DTD was fully positive as the wavelength of probe was slightly larger (less) than 2.35 μm (1.78 μm), whereas it became fully negative as the wavelength was located in the central part of the range of 1.78–2.35 μm. However, the dynamics was in turn evolved into an initial positive peak followed by a negative slowly decayed dynamics when the wavelength of probe was near 1.78 or 2.35 μm. Those diverse ultrafast dynamics has not been focused on and understood completely. Even some contradictory experimental results, measured on similar samples and under similar experimental conditions, have not been paid attention to yet, such as the experimental results reported in Refs. [1,8].

On the other hand, the quantitative analysis on the ultrafast dynamics was mainly based on three types of models, the biexponential decay [1,3,8–10,12], optical conductivity model in which either interband [5] or intraband [7] transition was solely taken into account and phenomenological models [2]. In principle, these models could not give accurate physical parameters unambiguously to describe real ultrafast processes occurred in graphene because they did not consider or incompletely considered the real physical processes so that the measurements of some physical parameters, such as momentum scattering time and lifetime of electron–hole recombination, have been absent or rare. The former was obtained mainly by theoretical calculation, and predicted to be in a large range of a few to a few hundreds of femtoseconds [2,7,16,17]. Meanwhile, it was also exhibited theoretically that the Fermi distribution of photoexcited carriers could be established within 100 fs [18]. Experimentally, Li et al. [5] even found the photoinjected carriers could be thermalized in 35 fs, implying a few scattering events enabling the photoinjected carriers thermalized if the scattering time of several to a few hundreds of femtoseconds is accepted [2,7,16,17]. It is evident that the experimental observation did not agree well with the theoretical prediction for the scattering time of carriers. The latter, the lifetime of electron–hole recombination, experimentally was reported rarely [6] except for theoretical calculations [19,20].

In this paper, we investigate ultrafast dynamics of photoexcited carriers in a CVD-grown monolayer graphene transferred on a quartz substrate, and find that DTD presents a first positive peak near zero-delay time, and then rapidly decays into a negative dynamics which recovers slowly back to the initial state. Such DTD is kept almost unchanged with increasing photoinjected carrier density but the amplitude of the positive and negative peaks is increased. A dynamic model of differential optical conductivity including both intra- and inter-band transitions is developed to simulate DTD for different scattering time, Fermi level, probe energy and photoinjected carrier density. The simulated results explain well the diversity of ultrafast carrier dynamics reported so far and our experimental results. Finally, the dynamic model is used best to fit our experimental results. The scattering time, lifetime of electron–hole recombination, and time constants of electron-optical phonon exchanging and optical phonon cooling are achieved. A striking sub-femtosecond hot-carrier scattering time is found, which is much less than the value of a few to a few hundred femtoseconds accepted currently.

2. Sample and experimental

The graphene sample studied here is grown on copper foil by CVD [21], and then transferred onto a thin quartz substrate as described in Ref. [22]. The sample is characterized with Renishaw in Via micro-Raman spectrometer at a laser wavelength of 514.5 nm and Perkin Elmer Lambda 900 absorption spectrometer. A Ti:sapphire self-mode-locked oscillator is used to study ultrafast carrier dynamics using transient differential transmission spectroscopy. The mode-locked laser pulse train has a repetition rate of 94 MHz, the central wavelength of 810 nm and the duration of ~80 fs. The laser pulse goes through a standard pump–probe setup and is split into a strong pump and weak probe with the intensity ratio of pump to probe larger than 10. The focused spot size of the pump and probe is about 50 μm in diameter and overlapped on sample. The pump and probe are perpendicularly polarized so that a polarization analyzer can be placed in front of photodetector to filter out the scattered pump light into the probe. The pump beam is modulated at a frequency of about 1.13 kHz by an optical chopper whose reference output synchronizes a lock-in amplifier which measures transient transmission change of the graphene induced by pump pulses.

3. Results and discussion

3.1. *Characterization of graphene grown by CVD*

A typical Raman spectrum is plotted in Fig. 1(a), and shows that the 2D peak is two times more intense than G peak, which implies that the graphene is monolayer. D peak is hardly observed, which imply the monolayer graphene has less defects [23]. G peak appears at 1587 cm^{-1}, which implies that the sample has a Fermi level of ~0.24 eV according to the doped density dependence of the position of G peak [23].

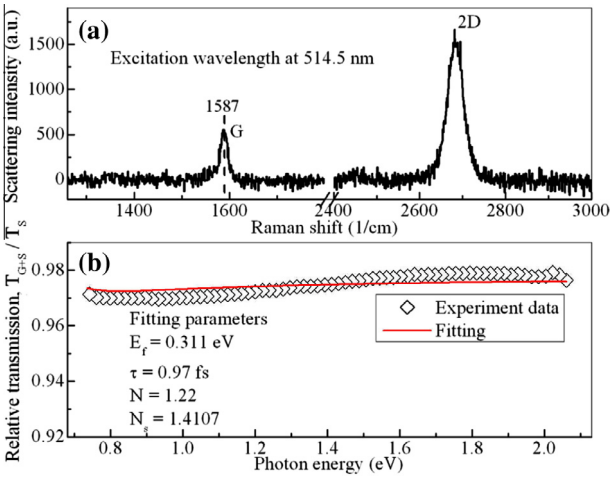

Fig. 1 – Raman (a) and transmission spectra (b) of the sample. Red line in (b) is the best fitting to experimental transmission spectrum with Eq. (1) described in text. (A colour version of this figure can be viewed online.)

Furthermore, the transmission spectrum of the sample on a quartz substrate is measured and plotted in Fig. 1(b), as the scattered points show. The transmission of the sample can be described by [1,6],

$$T(\omega) = \frac{T_{G+S}(\omega)}{T_S(\omega)} = \frac{1}{|1 + N\sigma(\omega)Z_0/(n_s+1)|^2}, \quad (1)$$

where $T_{G+S}(\omega)$ is the total transmission of graphene and substrate, while $T_S(\omega)$ is the sole transmission of the substrate. N and Z_0 are layer number of graphene and the vacuum impedance, respectively. The n_s is the refractive index of the substrate. The $\sigma(\omega)$ is the optical conductivity of monolayer graphene and can be written as [6,11],

$$\frac{\mathrm{Re}(\sigma(\omega))}{\sigma_0} = \frac{4k_BT}{\pi\hbar}\left[\ln\left(1+e^{E_F^h/k_BT}\right)+\ln\left(1+e^{E_F^e/k_BT}\right)\right]\frac{1/\tau}{\omega^2+1/\tau^2} + \frac{1}{2}\left[\tanh\left(\frac{\hbar\omega-2E_F^h}{4k_BT}\right)+\tanh\left(\frac{\hbar\omega-2E_F^e}{4k_BT}\right)\right], \quad (2)$$

where $\sigma_0 = e^2/(4\hbar)$ is the universal quantum conductivity. τ is the momentum scattering time. $E_F^e(E_F^h)$ is the electron (hole) Fermi energy with the relation $E_F^e = -E_F^h$ under thermal equilibrium condition. k_B and T are Boltzmann constant and absolute temperature, respectively.

The transmission spectrum in Fig. 1(b) can be best fit with Eq. (1) [1,6], as the solid line shows in Fig. 1(b). One can see the fitting is quite well and may be better if the dispersion of the substrate is taken into account. The best fitting gives parameters $E_f = 0.311$ eV, $N = 1.22$, $\tau = 0.97$ fs, and $n_s = 1.4107$. The $E_f = 0.311$ eV agrees well with $E_f = \sim 0.24$ eV given by Raman spectrum before. The $N = 1.22$ implies the sample is mainly monolayer, which also agrees well with the conclusion of monolayer graphene determined by Raman spectrum before. The $n_s = 1.4107$ agrees well with average refractive index of Quartz substrate in the range of 0.8–2.0 eV. The consistency between Raman and transmission spectra convinces us that the sample is mainly monolayer graphene and has a Fermi level between 0.24 and 0.31 eV. A middle value of 0.25 eV will be used in the following calculations. Finally, it is worth emphasizing that a sub-femtosecond momentum scattering time of $\tau = 0.97$ fs is given by the fitting, and smaller than the 2 fs reported in Ref. [6], which indeed shows a significant difference between our CVD-grown graphene and epitaxial graphene grown on 6H-SiC by thermal decomposition. We conjecture the difference may mainly originate from adsorbed impurities introduced in the chemical transfer processes of graphene from Cu foil onto a quartz substrate because such a difference is not reflected in Raman spectrum, but only in the transmission spectrum.

3.2. *Measurement of ultrafast dynamics in monolayer graphene*

Ultrafast dynamics of hot carriers is measured using degenerate near-infrared transient differential transmission spectroscopy. The measured spot of ~50 μm in diameter is located in a homogenous transparent area on the sample by means of an optical microscope to ensure a monolayer graphene measured. Fig. 2 shows DTD for different photoexcited carrier density. One can see that every transient profile presents a positive peak followed by a negative slow recovery dynamics. Femtosecond pump pulse first excites electrons into a state with a level of $E_p/2$ in conduction (E_p photon energy of pump pulse). The positive peak near time-delay zero mainly reflects just the state filling of the non-thermalized photoinjectd carriers. Then the photoinjected carriers undergo an ultrafast thermalizing process via electron–electron, electron–phonon and electron–impurity (not considered in theoretical calculations) interactions, while the sharp decay of the peak exhibits just the ultrafast thermalizing process. Finally, the thermalized carriers undergo a cooling and recombination process back to initial thermal equilibrium state, while the negative slow recovery dynamics in Fig. 2 just reflects the cooling and recombination processes.

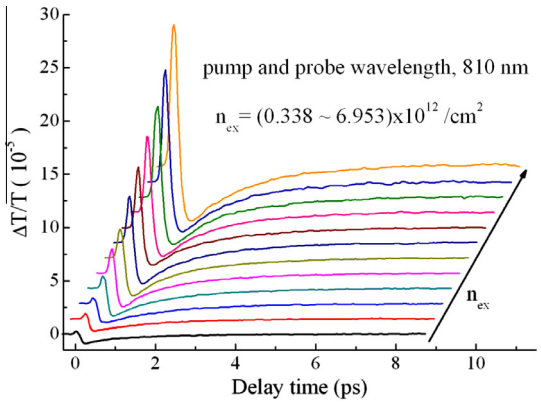

Fig. 2 – Photoexcited carrier-density dependence of ultrafast dynamics of CVD-grown monolayer graphene measure by degenerate pump–probe transient transmission spectroscopy at the central wavelength of 810 nm. n_{ex} denotes photoexcited carrier density. All curves are shifted for clarity. (A colour version of this figure can be viewed online.)

Diverse ultrafast dynamics in graphene mainly depends on the difference in time scale and strength of those dynamic processes for different graphene samples. Here it may deduce from Eq. (2) and the negative sign of the slow recovery dynamics that the contribution from the intraband transition to DTD is stronger than one from the interband transition in the relaxation process of thermalized carriers. One can also see that DTD is enhanced with increasing excited carrier density (n_{ex}) and the amplitude of the positive peak increases faster than that of the negative peak. Our DTDs are similar to some of DTDs reported in Refs. [12–15], but are distinct from the fully positive DTD reported in Refs. [1–4] and pure negative DTD reported in Refs. [6–9]. Why are DTDs so different or diverse in graphene? Are all DTDs reported previously and observed here reasonable? To answer these questions, we make simulations based on a recognized model of optical conductivity of monolayer graphene, as described in Eq. (2).

3.3. *Simulation of ultrafast dynamics*

The first term in Eq. (2) describes intraband transition which leads to transient absorption enhancement, while the second one depicts interband transition which results in transient absorption saturation. According to Eq. (1), transient differential transmission of monolayer graphene is proportional to $-\Delta[\mathrm{Re}(\sigma(\omega))]/\sigma_0$. Consequently, DTD in graphene should actually include two contributions from transient intraband and interband transitions. The appearance of DTD depends on the competition between the two contributions due to their opposite sign. Thus, in principle, DTD in monolayer graphene may be diverse. We demonstrate the diversity below by simulating DTD for different sample parameters and experimental conditions.

According to the physical picture discussed before on ultrafast dynamics, in the optical conductivity in Eq. (2), Fermi energy (E_F^e) and temperature (T) of electrons, should become time-dependent after photoinjected electrons (holes) into conduction (valence) band of graphene. Here the dynamics of electron temperature is assumed biexponentially decayed [1,3,8–10,12] because photoinjected electrons undergo first a thermalizing process and subsequent cooling process together with optical phonons, and thus is written as, $T(t) = T_0 + \Delta T_1 \exp(-t/\tau_{th}) + \Delta T_2 \exp(-t/\tau_{cool})$, where τ_{th} is a time constant which just measures the ultrafast thermalizing process of pump-injected carriers, while τ_{cool} describes the cooling time of the thermalized electron-optical phonon system. The ΔT_1 denotes the initial temperature of injected electrons, while ΔT_2 describe the initial temperature of thermalized electron-optical phonon system. The dynamics of Fermi energy may be described by the dynamics of electron–hole recombination based on the formula [6,11], $E_F^e(t) = \hbar v_F \sqrt{\pi(N_0 + n_{ex}\exp(-t/\tau_r)}$, where v_F is Dirac fermion velocity, N_0 is the doped electron density in graphene, while n_{ex} and τ_r are the photoinjected electron density and lifetime of electron–hole recombination, respectively. Substituting the dynamic Fermi energy and temperature into Eq. (2), a dynamic model of differential optical conductivity, $\Delta[\mathrm{Re}(\sigma(\omega,t))]/\sigma_0$, is developed. Based on the dynamic model, negative differential optical conductivity dynamics (proportional to DTD) is calculated for different doped density, scattering time, probe level and injected carrier density, and plotted in Fig. 3. The time constants used in the simulations, $\tau_{th} = 0.12$ ps, $\tau_{cool} = 1.8$ ps and $\tau_r = 1.2$ ps, are taken from the literature [1,6]. The ΔT_1 is the temperature of thermalized electrons and may be estimated from energy conservation [6], $U_e(T_0, N_0) + \Delta Q = U_e(T_0 + \Delta T_1, N_0 + n_{ex}) + U_h(T_0 + \Delta T_1, n_{ex})$, while the ΔT_2 is the initial temperature of thermalized equilibrium electron-optical phonon coupling system, and can also be estimated by energy conservation [11], $U_e(T_0, N_0) + \Delta Q - U_{phonon}(T_0 + \Delta T_2) = U_e(T_0 + \Delta T_2, N_0 + n_{ex}) + U_h(T_0 + \Delta T_2, n_{ex})$, where ΔQ denotes the graphene-absorbed energy from single pump pulses.

Fig. 3(a) shows the effect of momentum scattering time (τ) on DTD of monolayer graphene. One can discern that τ has significant influence on DTD. Small τ leads to the enhancement of negative peak and reduction of positive peak, which implies more frequent scattering events and thus more intense intraband transition. The negative peak decreases rapidly with increasing τ and vanishes almost as τ reaches 10 fs or above. At the moment, fully positive DTDs appear. Consequently, fully positive DTDs are possible, which may imply that the studied graphene may have a larger scattering time ($\tau \geqslant 10$ fs), as shown in Ref. [2], where a scattering time of ~40 fs at the probed level was calculated by taking account for electron-optical phonon scattering [2]. In contrast, the fully negative DTD reported in Ref. [8] cannot be explained physically because positive peak in DTD should always exist even if τ is reduced down to 0.5 fs, as Fig. 3(a) shows. Actually, it might be measured wrong because later the authors themselves reported fully positive DTD for the same graphene and similar conditions [24].

The effect of doped density (static Fermi level, E_f) on DTDs is calculated for a photoinjected carrier density of $n_{ex} = 3.375 \times 10^{12}/\mathrm{cm}^2$ and $\tau = 2$ fs at a probe level of 1.53 eV, and plotted in Fig. 3(b). One can see DTDs present the first positive peak followed by a negative slow recovery process for lower Fermi energy of $E_f < 0.4$ eV (far below the probed level of 1.53/2 = 0.765 eV). The amplitude of the negative peak becomes weak with raising E_f. As E_f rises up to 0.4 eV, the negative peak becomes insignificant. DTD becomes fully positive as E_f is larger than 0.4 eV but lower than the probed level (0.765 eV), as the DTDs indicated by $E_f = 0.5$–0.75 eV show. This agrees very well with a fully negative DRD (equivalent to fully positive DTD) reported in Ref. [5], where the Fermi level of monolayer graphene was claimed as ~0.4 eV which is close to the probed level (1.55/2 and 1.1/2 eV). With further increasing Fermi energy up to 0.8 eV which is slightly above the probed level, DTD becomes fully negative, as the green line with open circles shows in Fig. 3(b). This agrees very well with fully negative DTD reported in Refs. [6,7], where THz probe, whose energy is below Fermi level, was used to detect the interband transition near Dirac point and intraband transition.

Fig. 3(c) shows the probe-level (probe-photon energy) dependence of DTD for a given Fermi level of $E_f = 0.2$ eV, $\tau = 1$ fs and photoinjected carrier density of $n_{ex} = 3.375 \times 10^{12}/\mathrm{cm}^2$. One can see that DTD presents a positive peak followed by a negative slow recovery dynamics when the probe level is above 0.620 eV. The positive peak in amplitude increases with lowering the probe level from 2.065 to 0.620 eV, whereas the

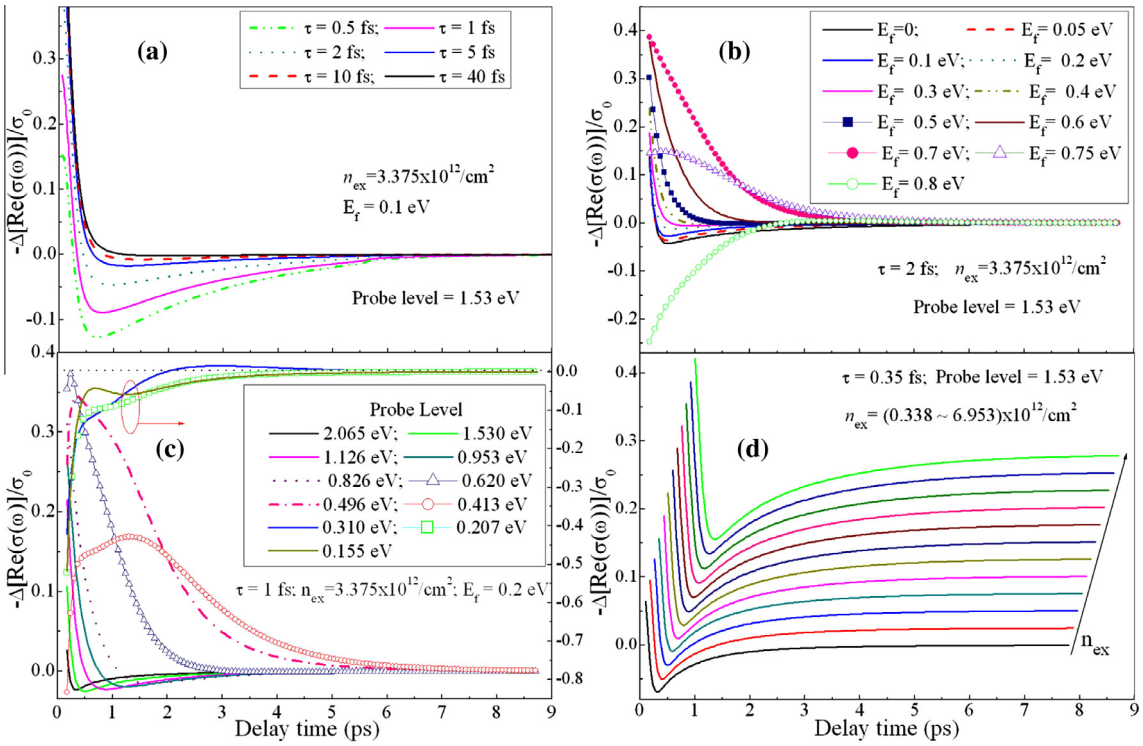

Fig. 3 – Simulations of ultrafast dynamics in monolayer graphene based dynamic model of differential optical conductivity at the probe of 810 nm for τ_{th} = 0.12 ps, τ_{cool} = 1.8 ps and τ_r = 1.2 ps. (a) The momentum scattering time (τ) dependence for a photoexcited carrier density of $n_{ex} = 3.375 \times 10^{12}/cm^2$. (b) Static Fermi level (E_f) dependence for τ = 2 fs and $n_{ex} = 3.375 \times 10^{12}/cm^2$. (c) The probe level dependence for τ = 1 fs, $n_{ex} = 3.375 \times 10^{12}/cm^2$ and E_f = 0.2 eV. (d) The photoexcited carrier density dependence for E_f = 0.25 eV and τ = 0.35 fs. (A colour version of this figure can be viewed online.)

change of the negative peak in amplitude is not monotonous. The amplitude of the negative peak first increases slightly as the probe level reduces starting from 2.065 eV and reaches a maximum at the probe level of 1.53 eV, as the green solid line shows in Fig. 3(c). Then, the amplitude decreases monotonously as the probe level further reduces from 1.53 eV, and approaches to zero at the probe level of 0.620 eV, as the line with open triangles shows in Fig. 3(c). This change of positive and negative peaks in amplitude reveals the competition between two contributions from the intra- and inter-band transitions. DTD becomes fully positive with further lowering the probe level from 0.620 eV to 0.412 eV. Those evolutions of DTD with the probe level agree well with experimental DTDs reported in Refs. [12–14] and theoretical calculations [25], where DTD was found fully positive for a range of lower probe level, whereas it became the first positive peak followed by a slow negative recovery dynamics for a range of higher probe level. However, there the occurrence of the slow negative recovery dynamics was explained by band-gap renormalization [12] and thermal diffusion and shrinkage of band separation caused by lattice heating [13,14] which was not confirmed experimentally. Actually, it may be explained well by the competition between inter- and intra-band transitions at different probe level, as shown in Fig. 3(c). With further reducing the probe level just across Fermi level, DTD is evolved into the first negative peak followed by a weak positive recovery dynamics, as the blue solid line shows in Fig. 3(c). Please note that the three dynamic profiles circled by an ellipse are scaled by right vertical axis. Then, DTD becomes fully negative as probe level is further reduced down to 0.207 and 0.155 eV, which again agrees well with DTDs detected by THz probe in Refs. [6,7].

Finally, the photoinjected carrier-density dependence of DTD is calculated and plotted in Fig. 3(d) for a probe level of 1.53 eV (810 nm), a low static Fermi energy of 0.25 eV and an excited carrier density range of $(0.338 \sim 6.953) \times 10^{12}/cm^2$, which are similar to the parameters in our experiment. One can see that DTD always presents a first positive peak followed by a negative slow recovery dynamics. The positive and negative peaks become intense with increasing n_{ex}. These features are well consistent with those of our experimental results shown in Fig. 2. In general, our calculations show that DTD in monolayer graphene indeed may be diverse, including fully positive, negative and the first positive then evolved into negative dynamics. The appearance of DTDs mainly depends on the position of the probed level with respect to Fermi level and scattering time τ. Fully positive DTD is possible as scattering time τ is larger (>10 fs) and/or the probed level is above but closer to Fermi level. In contrast, a fully negative DTD is also possible when the probed level is lower than Fermi level. Otherwise, a DTD with a first positive peak followed by a negative slow recovery dynamics should appear usually. Our calculations can almost explain all diverse ultrafast dynamics reported so far in the literature except two fully positive DRDs (equivalent

to fully negative DTD) reported in Refs. [10,11], and a fully negative DTD in Ref. [8], where the probed level was remarkably higher than Fermi level. Thus, DRD in Refs. [10,11] should present fully negative or a negative peak followed by a weak positive slow recovery dynamics. Actually, the two fully positive DRDs are also contradictory to the fully negative DRD reported in Ref. [5]. Based on the fully negative DRD, authors [11] claimed that sole intraband conductivity response was observed. To explain their fully positive DRD, they had to lower the temperature of electron–hole gas from ~4000 K to ~600 K which disagreed obviously with the true electron temperature of several thousands of Kelvins observed experimentally in Ref. [26]. Actually, the two fully positive DRDs might be measured incorrectly due to inappropriate setting of lock-in amplifier [27]. As for fully negative DTD reported in Ref. 8, it was indeed measured wrong and confirmed by the authors themselves later [24]. Correct DTD was fully positive, which agrees well with our calculations.

4. Analysis of experimental results

The dynamic model of differential optical conductivity, $\Delta[Re(\sigma(\omega,t))]/\sigma_0$, based on Eq. (2), is used to fit our experimental dynamics shown in Fig. 2 using Mathematica Software, where the dynamics of electron temperature and Fermi level is described in text before. The convolutions of the best fitting with auto-correlation function of laser pulse of 80 fs are plotted in Fig. 4 by solid lines, while scattered symbols denotes experimental data plotted in Fig. 2. One can discern the solid lines fit experimental data excellently. The best fitting gives out the carrier-density dependence of four time constants, such as scattering time τ, thermalizing time τ_{th} of photoinjected carriers, cooling time τ_{cool} of thermalized carrier-phonon coupling system and electron–hole recombination time τ_r. They are plotted in Fig. 5. The best fitting can give out unique solutions within a error of 10% for three time constants, τ, τ_{th} and τ_{cool}, but a doublet solution for τ_r. In other words, for a set of any initial values of the four parameters, the best fitting gives almost same solutions for τ, τ_{th} and τ_{cool}, but does one of two different possible solutions for τ_r if the fitting is converged. One can see from Fig. 5 that the two solutions for τ_r are in a time scale of ~0.2 ps

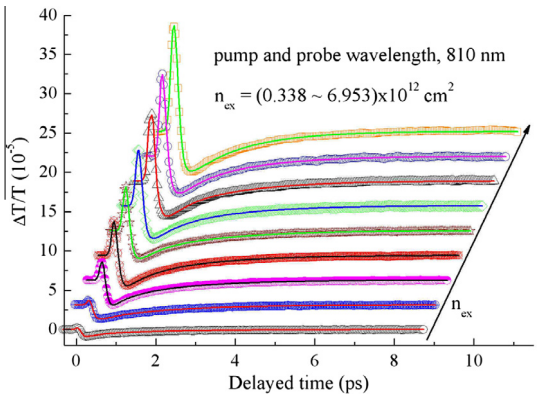

Fig. 4 – Best fitting of the measured ultrafast dynamics with dynamic model of differential optical conductivity for different photoexcited carrier density n_{ex}. (A colour version of this figure can be viewed online.)

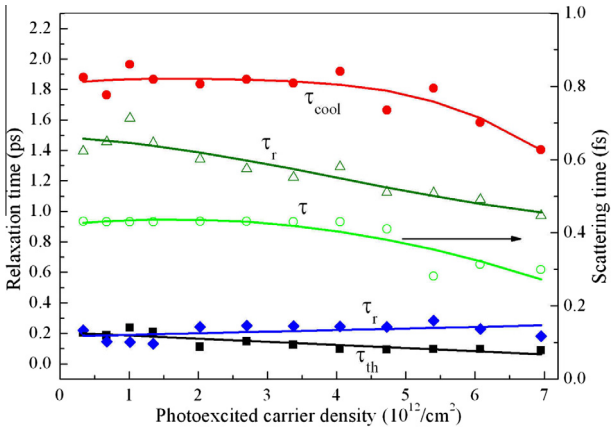

Fig. 5 – Photoexcited carrier-density dependence of various time constants retrieved by best fitting based on dynamic model of differential optical conductivity. τ, τ_{th}, τ_{cool} and τ_r denote the scattering, thermalizing, cooling and recombination time constants, respectively. Solid lines are the guide to eyes. (A colour version of this figure can be viewed online.)

and ~1.2 ps, respectively. All time constants are decreased with increasing photoinjected carrier density in present carrier density range of $<7.0\times10^{12}/cm^2$, which can be explained well by the enhancement of carrier-associated scattering interactions with increasing hot-carrier density. The thermalizing time constant τ_{th} is below 0.2 ps, while the cooling time constant τ_{cool} of thermalized carrier-optical phonon coupling system is below 2.0 ps. They are typical and consistent well with reported values [1,2,8]. Here we emphasize the scattering (τ) and recombination (τ_r) time constants because they were not or seldom reported experimentally. First, one can see a subfemtosecond scattering time obtained in Fig. 5. It is below 0.5 fs and slowly reduced with increasing hot carrier density. Such a small τ is achieved experimentally for the first time, and apparently smaller than the reported minimum of 2 fs [6], but supported by our transmission spectrum in Fig. 1(b) which gives out a scattering time of 0.97 fs. In a dynamic measurement, carrier density and temperature are raised significantly, and the latter can reach up to thousands of Kelvins [26]. It was already shown that the scattering time was temperature dependent and reduced with increasing temperature [28]. Therefore, it is reasonable for the scattering time of hot carriers to reduce down to ~0.5 fs from static scattering time of 0.97 fs. Second, doublet recombination times, τ_r = ~0.2 or ~1.2 ps, are obtained, as shown in Fig. 5. The reports on recombination time were sparse and controversial. Choi et al. [6] reported a recombination time of 1.2 ps by transient transmission of THz probe, while Lui et al. [26] reported on a recombination time of 0.1–0.2 ps by time correlation of photoluminescence from a higher level (>1.75 eV). Our doublet solutions agree well with two reports, respectively. However, which of our doublet solutions for τ_r is true here? We conjecture the shorter recombination time of ~0.2 ps is more reasonable because transient transmission of THz probe measured the relaxation dynamics of intraband carriers which was controlled by the recombination and cooling of hot carriers simultaneously.

As τ_{cool} is much larger than τ_r, the transmission dynamics of THz probe mainly reflects the cooling dynamics. Consequently, a larger relaxation time (assigned to recombination time) is given out. Photoluminescent dynamics mainly reflects recombination dynamics, and hence a shorter recombination time is given out. Furthermore, a more direct evidence to support our shorter lifetime solution is the direct view of hot carrier dynamics in conduction band by time-resolved photoemission spectroscopy [29]. Gierz et al. [29] indicated that hot carriers in whole conduction band disappeared at a delay time of 1 ps, and the dynamics of chemical potentials of hot electrons and holes showed a relaxation time of 0.13 ps. Those results support a recombination time of <1 ps. The origin of doublet solution for τ_r may result from a higher probed level where only the thermalizing dynamics of photoinjected carriers can be monitored sensitively, but the slow recombination dynamics cannot because thermalized Fermi-distributed carriers mainly are populated near the bottom of conduction band. The higher probed level is located at the tail of Fermi distribution where filling effect is very weak so that a negative slow recovery dynamics appears. In other words, the negative slow recovery dynamics following the positive peak in Fig. 2 mainly reflects cooling effect (intraband transition), whereas carrier filling (interband transition) is negligible.

5. Summary

We have studied ultrafast dynamics of CVD-grown monolayer graphene, and discussed the diversity of ultrafast dynamics in graphene. A dynamic model of differential optical conductivity is developed to simulate ultrafast dynamics in graphene. It is found that the diversity of ultrafast dynamics is possible because the ultrafast dynamics is dependent on multiple parameters, such as scattering time, static Fermi energy, probe level and photoexcited carrier density. A fully positive DTD is reasonable when scattering time is larger and/or probe level is above and closer to Fermi level. A dynamics with a positive peak followed by a negative slow recovery process may occur as probe level is far above Fermi level, whereas a fully negative DTD may appear when probed level is apparently below Fermi level. Contrarily, the full negative DTD and full positive DRD measured at higher levels than Fermi level is not reasonable physically. We also use the dynamic model of differential optical conductivity to best fit our experimental dynamic data, and have obtained the scattering time, thermalized time, recombination time and cooled time. They all are reduced with increasing excited carrier density, but recombination time almost keeps constant. A striking sub-femtosecond scattering time has been obtained for the first time, which is significantly smaller than the reported minimum of 2 fs measured in other graphene at room temperature, but supported by the sub-femtosecond scattering time given by data of our transmission spectrum. A sub-picosecond recombination time has also been obtained.

Acknowledgments

T.S. Lai thanks M.W. Wu for helpful discussions. This work was supported by National Natural Science Foundation of China under Grant Nos. 11274399 and 61078027, and National Basic Research under Grant Nos. 2010CB923200 and 2013CB922403 as well as doctoral specialized fund of MOE of China under Grant No. 20090171110005.

REFERENCES

[1] Dawlaty JM, Shivaraman S, Chandrashekhar M, Rana F, Spencer MG. Measurement of ultrafast carrier dynamics in epitaxial graphene. Appl Phys Lett 2008;92:042116.
[2] Wang HN, Strait JH, George PA, Shivaraman S, Shields VB, Chandrashekhar M, et al. Ultrafast relaxation dynamics of hot optical phonons in graphene. Appl Phys Lett 2010;96:081917.
[3] Zhao Xin, Liu ZB, Yan WB, Wu YP, Zhang XL, Chen YS, et al. Ultrafast carrier dynamics and saturable absorption of solution-processable few-layered graphene oxide. Appl Phys Lett 2011;98:121905.
[4] Tani S, Blanchard F, Tanaka K. Ultrafast carrier dynamics under a high electric field. Phys Rev Lett 2012;109:166603.
[5] Li T, Luo L, Hupalo M, Zhang J, Tringides MC, Schmalian J, et al. Femtosecond population inversion and stimulated emission of dense Dirac fermions in graphene. Phys Rev Lett 2012;108:167401.
[6] Choi H, Borondics F, Siegel DA, Zhou SY, Martin MC, Lanzara A, et al. Broadband electromagnetic response and ultrafast dynamics of few-layer epitaxial graphene. Appl Phys Lett 2009;94:172102.
[7] George PA, Strait J, Dawlaty J, Shivaraman S, Chandrashekhar M, Rana F, et al. Ultrafast optical-pump THz-probe spectroscopy of the carrier relaxation and recombination dynamics in epitaxial graphene. Nano Lett 2008;8(12):4248–51.
[8] Huang LB, Hartland GV, Chu LQ, Luxmi, Feenstra RM, Lian CX, et al. Ultrafast transient absorption microscopy studies of carrier dynamics in epitaxial graphene. Nano Lett 2010;10:1308–13.
[9] Newson RW, Dean J, Schmidt B, van Driel HM. Ultrafast carrier kinetics in exfoliated graphene and thin graphite films. Opt Express 2009;17(4):2326–33.
[10] Gao Bo, Hartland G, Fang T, Kelly M, Jena D, Xing HL, et al. Studies of intrinsic hot phonon dynamics in suspended graphene by transient absorption microscopy. Nano Lett 2011;11:3184–9.
[11] Dani KM, Lee J, Sharma R, Mohite AD, Galande CM, Ajayan PM, et al. Intraband conductivity response in graphene observed using ultrafast infrared-pump visible-probe spectroscopy. Phys Rev B 2012;86:125403.
[12] Shang JZ, Yu Ting, Lin JY, Gurzadyan GG. Ultrafast electron-optical phonon scattering and quasiparticle lifetime in CVD-grown graphene. ACS Nano 2011;5(4):3278–83.
[13] Shang JZ, Luo ZQ, Cong CX, Lin JY, Yu Ting, Gurzadyan GG. Femtosecond UV-pump/visible-probe measurements of carrier dynamics in stacked graphene films. Appl Phys Lett 2010;97:163103.
[14] Breusing M, Kuehn S, Winzer T, Mali'c E, Milde F, Severin N, et al. Ultrafast nonequilibrium carrier dynamics in a single graphene layer. Phys Rev B 2011;83:153410.
[15] Sun D, Wu ZK, Divin C, Li XB, Berger C, De Heer WA, et al. Ultrafast relaxation of excited Dirac fermions in epitaxial graphene using optical differential transmission spectroscopy. Phys Rev Lett 2008;101:157402.
[16] Tse WK, Hwang EH, Sarma SD. Ballistic hot electron transport in graphene. Appl Phys Lett 2008;93:023128.

[17] Hwang EH, Hu BYK, Sarma SD. Inelastic carrier lifetime in graphene. Phys Rev B 2007;76:115434.
[18] Sun BY, Zhou Y, Wu MW. Dynamics of photoexcited carriers in graphene. Phys Rev B 2012;85:125413.
[19] Rana F. Electron-hole generation and recombination rates for Coulomb scattering in graphene. Phys Rev B 2007;76:155431.
[20] Rana F, George PA, Strait JH, Dawlaty J, Shivaraman S, Chandrashekhar Mvs, et al. Carrier recombination and generation rates for intravalley and intervalley phonon scattering in graphene. Phys Rev B 2009;79:115447.
[21] Gao LB, Ren WC, Zhao JP, Ma LP, Chen ZP, Cheng HM. Efficient growth of high-quality graphene films on Cu foils by ambient pressure chemical vapor deposition. Appl Phys Lett 2010;97:183109.
[22] Li X, Zhu Y, Cai W, Borysiak M, Han B, Chen D, et al. Transfer of large-area graphene film for high performance transparent conductive electrodes. Nano Lett 2009;9(12):4359–63.
[23] Das A, Pisana S, Chakraborty B, Piscanec S, Saha SK, Waghmare UV, et al. Monitoring dopants by Raman scattering in an electrochemical top-gated graphene transistor. Nat Nanotechnol 2008;3(4):210–5.
[24] Huang LB, Gao Bo, Hartland G, Kelly M, Xing HL. Ultrafast relaxation of hot optical phonons in monolayer and multilayer graphene on different substrates. Surf Sci 2011;605:1657–61.
[25] Sun BY, Wu MW. Negative differential transmission in graphene. Phys Rev B 2013;88:235422.
[26] Lui CH, Mak KF, Shan Jie, Heinz TF. Ultrafast photoluminescence from graphene. Phys Rev Lett 2010;105:127404.
[27] Wang WF, Chen Ke, Wu JD, Wen JH, Lai TS. Influence of long lifetime absorption process on the measurement of ultrafast carrier dynamics. Acta Phys Sin 2011;60(11):117802.
[28] Strait JH, Wang HN, Shivaraman S, Shields V, Spencer M, Rana F. Very slow cooling dynamics of photoexcited carriers in graphene observed by optical-pump Terahertz-probe spectroscopy. Nano Lett 2011;11:4902–6.
[29] Gierz I, Petersen JC, Mitrano M, Cacho C, Turcu ICE, Springate E, et al. Snapshots of non-equilibrium Dirac carrier distributions in graphene. Nat Mater 2013;12:1119.